Distinct stages of the translation elongation cycle revealed by sequencing ribosome-protected mRNA fragments

Liana F Lareau, Dustin H Hite, Gregory J Hogan, Patrick O Brown

DOI: http://dx.doi.org/10.7554/eLife.01257

Cite as: eLife 2014;10.7554/eLife.01257

Received: 19 July 2013
Accepted: 8 May 2014
Published: 9 May 2014

Distinct stages of the translation elongation cycle revealed by sequencing ribosome-protected mRNA fragments

Liana F. Lareau*†[1], Dustin H. Hite*, Gregory J. Hogan, and Patrick O. Brown

Department of Biochemistry, Stanford University School of Medicine; and Howard Hughes Medical Institute

*These authors contributed equally

†For correspondence: lareau@berkeley.edu

[1]Current address: California Institute for Quantitative Biosciences, University of California, Berkeley

During translation elongation, the ribosome ratchets along its mRNA template, incorporating each new amino acid and translocating from one codon to the next. The elongation cycle requires dramatic structural rearrangements of the ribosome. We show here that deep sequencing of ribosome-protected mRNA fragments reveals not only the position of each ribosome but also, unexpectedly, its particular stage of the elongation cycle. Sequencing reveals two distinct populations of ribosome footprints, 28-30 nucleotides and 20-22 nucleotides long, representing translating ribosomes in distinct states, differentially stabilized by specific elongation inhibitors. We find that the balance of small and large footprints varies by codon and is correlated with translation speed. The ability to visualize conformational changes in the ribosome during elongation, at single-codon resolution, provides a new way to study the detailed kinetics of translation and a new probe with which to identify the factors that affect each step in the elongation cycle.

Introduction

To accomplish the huge task of translation elongation – in each cycle, accurately incorporating a new amino acid into a nascent peptide every 1/6th of a second, then moving precisely three nucleotides along the mRNA template – the ribosome undergoes a series of major structural rearrangements (Figure 1) (reviewed in Chen et al., 2012; and Noeske and Cate, 2012). During the initial decoding step of elongation, aminoacylated tRNAs are delivered to the decoding site (A site) as part of a ternary complex with EF-Tu (in prokaryotes) or the orthologous eEF1A (in eukaryotes). When the anticodon of one of these aminoacylated tRNAs is able to base-pair stably with the specific mRNA codon in the decoding site (A site), a new peptide bond is formed between the nascent polypeptide and the specified amino acid. The ribosome then undergoes a massive rearrangement in which the ribosomal subunits rotate relative to each other (Frank and Agrawal, 2000; Zhang et al., 2009). Along with this rotation, the A and P site tRNAs move from 'classic' to 'hybrid' states: the anticodon ends stay in their original A and P sites and the acceptor ends move to the P and E sites (Moazed and Noller, 1989; Munro et al., 2007). This rotated state of the ribosome undergoes additional conformational changes in preparation for translocation (Fu et al., 2011; Zhang et al., 2009). The ribosome can fluctuate between rotated and non-rotated states until EF-G (eEF2 in eukaryotes) binds and stabilizes the rotated ribosome (Agirrezabala et al., 2008). GTP hydrolysis by EF-G then promotes translocation of the mRNA along the ribosome, coupled to a large intrasubunit rotation of the 30S head (Ratje et al., 2010), after which the ribosome subunits rotate back to a closed formation for the next cycle (Gao et al., 2009). Structural and biochemical studies have revealed many of the atomic-level changes that allow this complicated process to occur (Pulk and Cate, 2013; Tourigny et al., 2013; Zhou et al., 2013), and new details continue to emerge, reshaping models, raising new questions and leaving other questions still unanswered.

Recently, "ribosome profiling" by high-throughput sequencing of ribosome-protected fragments has provided a powerful tool for identifying the position of

ribosomes on mRNAs across the entire transcriptome (Ingolia et al., 2009). Cell lysates are treated with nuclease to degrade all mRNA not physically protected by ribosomes, and the ribosome-protected fragments are extracted, sequenced, and mapped back to the genome to show ribosome positions, revealing the overall translation level of each gene as well as the distribution of ribosomes along the mRNA. Nucleotide-level precision of ribosome positions is possible because of the very consistent size of ribosome footprints in the conditions assayed. The authors of the method used a nuclease protection assay to establish that, in yeast treated with the elongation inhibitor cycloheximide, each ribosome protects a footprint of 28 nucleotides (nt), confirming earlier reports (Steitz, 1969; Wolin and Walter, 1988).

While performing ribosome profiling experiments in *Saccharomyces cerevisiae,* we serendipitously noticed a population of smaller ribosome-protected fragments. To better capture these fragments and to investigate their origins, we revised the ribosome profiling protocol originally established by Ingolia *et. al*. Our experiments revealed that, in the absence of cycloheximide, the small ribosome-protected fragments were abundant, consistent with an early observation of short ribosome footprints in the absence of cycloheximide (Wolin and Walter, 1988). We show here that the small fragments originate from ribosomes in a conformation distinct from that previously observed in the presence of cycloheximide. The ability to discern distinct ribosomal structural states by ribosome profiling has given us insight into how codon, tRNA, and amino acid identity and translational speed relate to ribosome structure. This additional dimension of ribosome profiling data will provide a valuable new layer of molecular and mechanistic information, at codon resolution, for future studies of translation.

Results

Ribosomes can protect two distinct mRNA fragment sizes

We began our investigation of ribosome footprint size by isolating ribosome-protected mRNA fragments from yeast using a modified ribosome profiling procedure. The standard ribosome profiling protocol includes a size selection for

RNA fragments of around 28 nt. To eliminate the bias against smaller fragments, we broadened the initial size range and selected RNA fragments between 18 and 32 nt after RNase I digestion. By selecting fragments in this broader size range, and, importantly, by carrying out the entire procedure in the absence of cycloheximide or other inhibitors, we observed two clearly distinct, abundant populations of ribosome-protected mRNA fragments ("footprints"), 28-30 nt and 20-22 nt long. We visualized fragment lengths and positions with a three-dimensional "metagene" representation: sequence reads representing the ribosome-protected fragments from all expressed genes were aligned relative to the start codon of the corresponding gene and tallied by fragment length and position to show the average pattern of translation along all annotated coding regions (Figure 2, A, B and C; Figure 2—supplement 1).

We found overwhelming evidence that both populations of fragments came from translating ribosomes. The 21 and 28 nt fragments were both found almost entirely within annotated coding regions (CDS) and not in 5' or 3' UTRs; 98.3% - 99.7% of mappable 21 nt fragments, and 96.5% - 99.6% of mappable 28 nt fragments, mapped within the annotated CDS in three replicates (Figure 2D). Both populations also showed the 3-nucleotide periodicity expected of fragments originating from elongating ribosomes (Figure 2E). We conclude that fragments of both sizes are footprints of translating ribosomes.

The 5'-most peaks in the metagene represent ribosomes with the start codon in the P site and the second codon in the A site (Ingolia et al., 2009; Kapp and Lorsch, 2004). Using this as a reference for phasing all the footprints, we inferred that for ribosomes with a given codon in the A site, small and large footprints generally had the same 5' ends positioned 15-16 nt upstream of the A-site codon, and differed at their 3' ends: extending 2-3 nt beyond the A-site codon in the small footprints and 10 nt beyond the A-site codon in the large footprints, respectively (Figure 2F).

Different elongation inhibitors stabilize distinct conformations and bias the footprint size distribution

During elongation, at each codon, the ribosome cycles through a stereotyped sequence of steps as it incorporates the specified amino acid and translocates to the next codon. These steps are accompanied by major rearrangements of the ribosome structure, including a rotation of the large subunit relative to the small subunit upon peptide bond formation. We hypothesized that the non-rotated, pre-peptide-bond ribosomes and rotated, post-peptide-bond ribosomes might protect different lengths of mRNA, and that the two resulting footprint sizes might, therefore, represent these two conformations.

To determine what footprint sizes were protected by ribosomes in distinct stages of elongation, we performed ribosome profiling on yeast treated with inhibitors that block different steps of the cycle. Cycloheximide is an elongation inhibitor that binds to the E site of ribosomes, preventing the E site tRNA from leaving the ribosome. When cycloheximide was added to the yeast immediately before harvest and was present throughout lysis and RNaseI treatment, the most prevalent footprints were 28-30 nt long and were distributed along the coding sequence with a 3-nt periodicity (Figure 3A, 3B, and 3C; Figure 3—supplement 1). Apart from a distinct peak at the start codon, there were very few 20-22 nt footprints.

Our data confirmed previous evidence that the ribosome predominantly protects a 28 nt footprint in the presence of cycloheximide, and suggest that cycloheximide stabilizes one stage of the elongation cycle. Previous work shows that cycloheximide bound alongside a tRNA in the E site prevents either the incorporation of the next aminoacylated tRNA in the A site or peptide bond formation (Schneider-Poetsch et al., 2010). In either case, it is expected to trap the ribosome in a non-rotated conformation, suggesting that the non-rotated conformation protects 28-30 nt of mRNA.

We next conducted ribosome profiling experiments using yeast treated with anisomycin, an elongation inhibitor that binds to the peptidyl transferase center (Grollman, 1967; Hansen et al., 2003). We observed almost exclusively small

143 footprints in yeast treated with anisomycin (Figure 3D, 3E, and 3F; Figure 3—
144 supplement 1). By comparison to the effects of cycloheximide treatment, we
145 inferred that anisomycin stabilizes a distinct conformation of the ribosome that
146 protects 20-22 nt of mRNA. Although anisomcyin's precise mechanism is not
147 characterized, it has higher affinity for post-translocation ribosomes than for pre-
148 translocation, cycloheximide-treated ribosomes, suggesting that it preferentially
149 binds a ribosome conformation distinct from that stabilized by cycloheximide
150 (Barbacid and Vazquez, 1974, 1975). Lincomycin and other antibiotics that bind the
151 peptidyl transferase center induce translocation, and lincomycin-treated ribosomes
152 prefer a rotated conformation in *in vitro* FRET experiments (Ermolenko et al., 2013;
153 Fredrick and Noller, 2003). It is possible that anisomycin acts similarly to stabilize a
154 rotated conformation.

155 We have thus demonstrated that two distinct ribosome conformations can be
156 stabilized using elongation inhibitors. Stabilization of distinct conformations by two
157 drugs resulted in a nearly complete reciprocal bias in the size of ribosome
158 footprints, providing evidence that large and small footprints originate from distinct
159 ribosomal conformations. We hypothesize that each ribosome cycles through both
160 conformations, protecting first a large footprint and then a small footprint at each
161 codon. The footprints identified by high-throughput sequencing in a ribosome-
162 profiling experiment represent a deep sampling of ribosomes in different states, and
163 thus the ratio of large to small footprints in untreated cells could show, at single-
164 codon resolution, how many ribosomes are in each stage of elongation.

165 *Increased decoding time produces more large footprints*

166 To enrich for ribosomes in a single, defined stage of the elongation cycle, we
167 induced conditions expected to result in the depletion of a specific aminoacyl-tRNA
168 and thus to increase the decoding time when the cognate codon is in the A site. We
169 treated yeast with 3-amino-1,2,4-triazole (3-AT), an inhibitor of histidine
170 biosynthesis, to create a specific shortage of His-acylated tRNA and cause ribosomes
171 to pause on histidine codons (Figure 4A). We would therefore expect ribosomes to

accumulate at histidine codons in a pre-peptide-bond conformation. Estimating codon-specific occupancy as described in more detail below, we found that the shortage of His-tRNA dramatically increased the relative abundance of large footprints from ribosomes with His codons in the A site, with minimal effect on the abundance of small footprints (Figure 4B and 4C; Figure 4 – figure supplement 1). During the decoding phase of elongation, before peptide bond formation, the ribosome is in a non-rotated conformation (Frank and Agrawal, 2000; Gao et al., 2009); these results therefore strongly suggest that the decoding phase of elongation (the non-rotated conformation) is represented by large footprints.

The footprint size distribution varies by codon

Recently, ribosome profiling has revealed that translation speed varies systematically by codon (Dana and Tuller, 2012; Stadler and Fire, 2011; Tuller et al., 2010); we hypothesized that there might be distinct codon-specific effects on the rate of the two distinct phases of elongation represented by small and large footprints.

Using data from untreated cells, we calculated the number of large and small footprints corresponding to ribosomes with a given codon in the A site, for each codon position in the yeast transcriptome. Large footprints were defined as 28 or 29 nt and small footprints were defined as 20, 21, or 22 nt with 5' ends positioned relative to the inferred A site as depicted in figure 2F. We found substantial variation in the characteristic length distribution between codons: small footprints ranged from 38 ± 12% (UUU) to 87 ± 9% (CGG) of the total footprints for a given codon identity, averaged across three replicates.

To explore this codon effect, we computed the relative occupancy of each of the 61 sense codons in the A site. We started by considering an individual gene and calculated the over- or underrepresentation of footprints at each codon position compared to the average for all codon positions in that gene, including both small and large footprints (an example from a highly expressed gene is shown in Figure 5A). After performing this computation for every gene, we averaged these

multipliers across all occurrences of a given codon in the genome to provide the "relative occupancy" for that codon, representing, on a relative scale, how frequently we observed ribosomes with that codon positioned at the A site. The relative occupancies varied over a five-fold range, from 0.48 ± 0.04 (GGU) to 2.6 ± 0.67 (CCG) (unitless, average of three replicates) and were highly correlated between independent replicates (Figure 5B). As a control, we also analyzed the occupancy based on the codon one position 3' of the A site, which has not yet entered the decoding site. We found that the range of occupancies relative to the codon in the A site was much broader than the range of occupancies relative to the next codon, suggesting that the A-site occupancies reflect an aspect of translation, not merely confounding factors such as biases in fragment capture (Figure 5 — supplement 1).

Codon-specific differences in ribosome occupancy could have been driven by variation in small footprint counts, variation in large footprint counts, or both, potentially revealing the variability of each stage of elongation. We inferred the relative abundance of ribosomes in each state at each codon using a model similar to the one we used to estimate overall relative occupancy, but considering counts of either small or large footprints separately (Figure 5A). As with overall occupancy, the relative abundances of small footprints and the relative abundance of long footprints were both highly correlated between replicates (Figure 5C and 5D). This suggests that codon identity affected both the pre-peptide-bond and post-peptide bond stages of elongation. However, the effect of codon identity on the inferred duration of these two phases of the elongation cycle was distinct: the codon-specific relative abundances of small and large footprints were almost uncorrelated (Spearman's r = 0.11, average of three replicates). This led us to search for physical correlates of the codon-specific differences.

Relative occupancy is related to amino acid polarity and codon:tRNA interactions

We found that a major and unexpected determinant of the abundance of footprints from each conformation was the identity of the amino acid encoded by the A-site codon. We found a much greater density of small footprints at codons

encoding smaller, polar amino acids than at codons encoding large, aromatic amino acids. The relative abundance of small footprints at codons encoding a given amino acid was correlated with measures of polarity of the cognate amino acid, such as the K_d of transfer of side chains from vapor to water (Spearman's r = -0.75 when grouped by amino acid, r = -0.58 by codon, Figure 6A), while the relative abundance of large footprints showed no correlation to amino acid polarity (Spearman's r = 0.11 by amino acid, r = 0.02 by codon) (Wolfenden, 2007). These data strongly suggest that the chemical properties of the amino acid specified by the codon in the A site affect the stability of the rotated, post-peptide-bond conformation of the ribosome. We hypothesize that interactions between the ribosome and polar amino acids acylated to the A-site tRNA can slow translocation substantially.

Many factors have been proposed to affect translation speed at a given codon, particularly tRNA abundance. In yeast, the number of genes encoding a specific tRNA has been shown to be highly correlated with both codon usage and cellular tRNA concentrations (Percudani et al., 1997). A related measure of codon optimality is the tRNA adaptation index (tAI), which attempts to rank codons in translational efficiency by accounting for tRNA copy number, wobble pairing constraints, and codon usage (dos Reis et al., 2004). We found that the relative occupancy per codon was only weakly correlated with tAI and with tRNA genomic copy number (Spearman's r = -0.39 and -0.28, respectively; average of three replicates) and that the tAI was not particularly correlated with the relative abundance of either small footprints or large footprints (r = –0.34 and r = –0.20, respectively; average of three replicates). Thus, unexpectedly, codon "optimality", as represented by the tAI, does not appear to be a major determinant of relative ribosome occupancy under the conditions tested here. The 3-AT data show that in extreme cases, limited supplies of the tRNA cognate to the A-site codon slows translation during the large-footprint stage. In contrast, our overall results in untreated yeast suggest that the differences in abundance among tRNAs in wild-type cells have only a minor effect on relative ribosome occupancy of the cognate codons under optimum growth conditions.

We also investigated the relationship between wobble base pairing, relative occupancy, and the density of large and small footprints. Wobble base pairing at the A site has recently been linked with slowed elongation in humans and worms (Stadler and Fire, 2011). We compared codons with perfect Watson-Crick complementarity versus the synonymous codons that pair imperfectly with the same tRNA (Johansson et al., 2008). While we found no consistent trend toward increased occupancy at wobble-paired codons, we observed notably higher occupancy on a subset of wobble-paired codons comprising proline CCG (G-U base pairing), leucine CUG (G-U), and arginine CGA (A-I) (Figure 6B). For these three wobble codon outliers, we see a dramatic increase in short footprints, representing post-decoding stages of translation (Figure 6C and 6D). The arginine CGA codon is known to be a strong inhibitor of translation in yeast, and its inhibitory effect is due more to wobble decoding than tRNA abundance and may include interactions after the initial decoding (Letzring et al., 2010). Our data confirm that CGA is indeed one of the most slowly translated codons, and its high relative occupancy is due to increased abundance of small footprints, suggesting that its slow elongation is primarily due to a prolonged post-decoding stage. Overall, the abundance of footprints from each step of elongation was clearly affected by several distinct codon-specific features with sometimes synergistic and sometimes opposing effects.

Discussion

A ribosome must cycle through a series of consecutive associations with mRNA to decode the message one codon at a time. The stability of the ribosome-mRNA association allows one to observe precisely where ribosomes reside on transcripts – down to the codon being decoded – by isolating and sequencing ribosome-protected mRNA fragments. We were quite surprised to discover that the ribosome protects two different footprint sizes (28-30 nt and 20-22 nt), as the original ribosome profiling experiments and nuclease protection assays only captured the longer footprints (Ingolia et al., 2009). The difference is explained by the experimental conditions: the small footprints were revealed only after we left out cycloheximide, a translation inhibitor commonly used to stabilize ribosomes on

mRNA for ribosome profiling. Indeed, early study of ribosome pausing found that when cycloheximide was omitted, 20-24 nt footprints accumulated in addition to the larger footprints they saw from cycloheximide-treated ribosomes (Wolin and Walter, 1988). As in our own experiments, the small and large footprints they observed had the same 5' terminus and differed at the 3' end.

We propose that the two footprints sizes originate from two ribosome conformations corresponding to different stages of elongation: large footprints from non-rotated ribosomes during the decoding stage before peptide bond formation, and small footprints from rotated ribosomes during the translocation stage after peptide bond formation. Additional biochemical and structural studies will be required to pinpoint the exact stages of elongation and ribosome conformations responsible for the two footprint sizes. It is not clear which of the known conformational changes during the elongation cycle are most relevant: the inter-subunit rotation after peptide bond formation, the intra-subunit swivel of the 30S head during translocation, or smaller rearrangements such as movement of the L1 stalk.

As for the physical origin of the small and large mRNA fragments, crystal structures of rotated and non-rotated ribosomes show that mRNA accessibility is not likely to be dramatically different between the two conformations (Ben-Shem et al., 2011; Ben-Shem et al., 2010). RNAse I may be small enough to penetrate into the mRNA entrance channel and cleave the mRNA just two nucleotides from the A site. Alternately, the ribosome itself may be more susceptible to RNAse degradation in the rotated conformation, allowing ribosomal RNA cleavage that in turn enables RNAse I to access the mRNA entrance channel, yielding a smaller mRNA footprint. Importantly, however, both small and large footprints have also been observed in wheat germ extract treated with micrococcal nuclease, indicating that the two footprint sizes are neither species- nor nuclease-specific (Wolin and Walter, 1988).

We hypothesize that the relative abundance of large and small footprints reflects the relative duration of different stages of elongation at each codon. (We use

the A site codon by default in this discussion, though in principle we could compile results based on the codon in the P site or any other frame of reference.) Comparing our relative occupancy values to an estimated bulk elongation rate of 5.6 amino acids per second (Ingolia et al., 2011), our model would predict variation in average codon elongation time from as little as 0.08 seconds (GGU) to as much as 0.5 seconds (CCG). A number of caveats apply to this interpretation, and any hypotheses must be pursued with complementary approaches. Ribosome footprint data have inherent biases from ligation and other steps of the library preparation. Further, the overall balance of small and large footprints varied between replicates, leaving open the question of which conformation is more populated *in vivo*. Some variability arises from the mRNA fragment isolation. In this work, we chose size markers of 18 and 32 nt, but size selection from polyacrylamide gel is imprecise. (This choice also limits what we can observe: recent work found distinct 16 nt fragments from ribosomes stalled on truncated mRNAs (Guydosh and Green, 2014)). The size distribution may also reflect differential efficiency of library preparation from smaller or larger fragments. Nonetheless, although the overall ratio of small to large footprints varied, the codon-specific variation in this ratio was robust.

Our results also highlight the effects of harvest methods and inhibitors such as cycloheximide on footprint distribution. Ribosomes are depleted from the first 50 codons when yeast are harvested by the procedure we used without inhibitors. We interpret this as evidence that elongation continues for around 10 seconds after initiation ceases during the harvest process. Because the selective depletion of ribosomes from this part of the mRNA could enrich for special cases, we excluded the first 50 codons from our analysis of per-codon footprint distributions. Different harvest methods had large effects on the precise footprint locations even when the overall translation per gene was highly reproducible (data not shown). Similarly, the average occupancies per codon with and without cycloheximide were surprisingly uncorrelated (Spearman's r = 0.02, comparing the average of three untreated samples and the average of two cycloheximide-treated samples), though the total footprints per gene correlated quite well (Spearman's r = 0.97 between the average

fpkm in three untreated samples and the average fpkm in two cycloheximide-treated samples). Ribosomes in different positions may be differentially affected either by the drug treatment or by runoff elongation during harvest without inhibitors. In either case, some ribosomes may halt while others undergo several more rounds of elongation.

There are many potentially rate-controlling steps of elongation and many factors necessary for each cycle, including aminoacylated tRNA and elongation factors eEF1, eEF2, and the yeast-specific eEF3 (Kapp and Lorsch, 2004). For example, interactions between the tRNA anticodon and the mRNA codon, the tRNAs and the ribosome, the amino acids and the peptidyl transferase center, and the nascent peptide and the tunnel, as the tRNAs move through the A, P and E sites, can all presumably affect the speed of each step. Thus, the speed of each elongation cycle is expected to be influenced by codon, tRNA, and amino acid identity.

One of the surprising aspects of this study is that tRNA abundance or codon optimality failed to predict variation in observed ribosome occupancy and, further, that much of the variation in codon-specific occupancy was in the steps following decoding and peptide bond formation. Biochemical evidence suggests that evolution has tuned tRNA sequence and modifications to balance the contributions of amino acid identity, codon pairing strength, and tRNA structure to binding affinity of a given tRNA, such that most aminoacylated tRNAs have similar affinity to ribosomal A sites (Dale et al., 2009; Olejniczak et al., 2005; Shepotinovskaya and Uhlenbeck, 2013). While this affinity tuning is a plausible result of selection for fidelity in decoding, ribosome profiling has revealed a lack of uniformity both in decoding and post-decoding steps. Once the interactions that determine the codon-specific rate of decoding are decoupled and replaced by a new set of codon-specific interactions in the subsequent steps of elongation, the great diversity in physical properties of amino acids and in the intrinsic stability of the codon-anticodon interaction may lead to wide variation in the kinetics of post-decoding steps.

New methods for high-throughput measurement of translation have led to renewed interest in modeling the constraints on coding sequence and the effects of codon choice on translation efficiency (Charneski and Hurst, 2013; Dana and Tuller, 2012; Plotkin and Kudla, 2011; Shah et al., 2013; Tuller et al., 2010). The ability to distinguish ribosome conformations at codon resolution now allows us to map these effects to specific phases of the elongation cycle, initiation or termination. Future *in vivo* and *in vitro* experiments using this approach to monitor the decoding and translocation steps at each codon should provide new precision in dissecting the mechanisms by which mRNA sequence, core translation factors and regulatory factors control initiation, elongation, and termination of translation.

Materials and methods

Yeast strains and growth conditions

For all experiments, excluding 3-AT drug treatment experiments, BY4741 was grown overnight in YPD at 30 °C; two 500mL cultures of YPD were inoculated from the overnight culture to an OD_{600} of ~0.2. For experiments involving 3-AT, S288C was grown as above in SC-His media at 30 °C. Cells were then grown to mid-log phase, OD_{600} ~0.6, prior to harvest. (Strain information: BY4741 derived from S288C: MATa his3Δ1/his3Δ1 leu2Δ0/leu2Δ0 lys2Δ0/LYS2 MET15/met15Δ0 ura3Δ0/ura3Δ0. S288C: MATa SUC2 gal2 mal mel flo1 flo8-1 hap1.)

Cells were harvested by filtration at room temperature and then quickly frozen in liquid N_2. Resulting cell pellets were then pulverized using a MM301 Retsch mixer mill at 30 hz for 3 minutes. All chambers and tubes were pre-frozen in liquid N2 or dry ice. Approximately 400-500 µL of cold lysis buffer (20 mM Tris pH 8.0, 140 mM KCl, 1.5mM $MgCl_2$, 1% Triton) was added to cell powder. Resulting lysates were pre-cleared by centrifugation at 2,000 rpm for 5-10 minutes at 4 °C. Lysate was transferred to a clean pre-chilled tube and further clarified by centrifugation at 20,000 *g* for 10 minutes at 4 °C. Lysate was then stored at -80 °C until RNase digestion.

For the cycloheximide experiments, cycloheximide was added to cells prior to harvest at 100 μg/mL and was also present at 100 μg/mL in the lysis buffer. For the anisomycin experiment, anisomycin was added to mid-log cells at 100 μg/mL and cells were allowed to grow for an additional 30 minutes prior to harvest. Anisomycin was also present at 100 μg/mL in the lysis buffer. For the 3-AT experiments, 3-amino-1,2,4-triazole was added to mid-log cells to reach a final concentration of 100mM, then cells were grown with shaking for 10 and 60 min prior to harvest.

RNase digestion and monosome isolation

RNase digestion and monosome isolation were performed similar to Ingolia et. al. (Ingolia et al., 2012; Ingolia et al., 2009). Cell lysate (~800 μg total RNA measured by Nanodrop) was allowed to thaw on ice. 600 U of RNase I (Life Technologies, AM2294) was added to cell lysate and placed on a nutator at room temperature for 1 hour. A second cell lysate served as an undigested control; 120 U of SUPERase-In was added and placed on a nutator as above. Linear 10%-50% sucrose gradients were prepared using a BioComp Gradient Master (Biocomp Instruments) according to manufacturer's instructions. Sucrose was dissolved in 20 mM Tris pH 8.0, 140 mM KCl, 5 mM $MgCl_2$, 0.5 mM DTT, 20 U/mL SUPERase-In; 100 μg/mL cycloheximide or 100 μg/mL anisomycin were added to buffer for corresponding experiments. After RNase digestion, lysate was added to the top of gradients and sedimented at 35,000 rpm in a SW41 rotor for 3 hours.

Gradients were fractionated at 0.17 mm per second using the BioComp Gradient Master while the A_{260} was continuously monitored. Fractions corresponding to the monosome peak were collected and pooled. RNA was then purified using a miRNeasy Mini kit from Qiagen (Qiagen cat# 217004) as per manufacturer's instructions.

Library preparation and high-throughput sequencing

Ribosome footprint libraries were prepared similar to Ingolia et.al. (Ingolia et al., 2012). Purified RNA was separated on a 15% TBE-Urea gel. RNA oligonucleotides of 18 and 34 nucleotides were run side by side with isolated RNA and used as size markers to cut RNA of desired size for gel extraction. Size-selected RNA fragments were then treated with polynucleotide kinase to remove the 3' phosphate. After isopropanol precipitation, dephosphorylated fragments were ligated to Universal miRNA cloning linker from New England Biolabs (cat# S1315S). Ligated fragments were separated from excess linker by gel electrophoresis on a 15% TBE-Urea gel. After gel extraction, ligated fragments were then reverse transcribed using SuperScript III from Life Technologies (cat# 18080-085) according to manufacturer's instructions. Reverse transcriptase reactions were primed with 1 µL of 1.25 µM NI-NI-9 primer (Supplementary file 1). Additionally 20 U of SUPERase-In was added to each RT reaction. Reactions were incubated at 48 °C for 30 minutes.

After reverse transcription, RNA template was removed by the addition of 2.2 µL of 1 N NaOH and incubation at 98°C for 20 minutes. After precipitation, cDNA was separated from excess primer by gel electrophoresis on a 5% TBE-Urea gel. cDNA was then circularized using CircLigase ssDNA ligase from Epicentre (cat# CL4115K) according to manufacturer's instructions. After circularization, 5 µL of the circularization reaction was added to 1 µL of pooled ribosomal subtraction oligos (Supplementary file 1), 1 µL of 20x SSC, and 3 µL of water. Each sample was then denatured for 90 seconds at 100°C and then annealed to 37°C. MyOne Streptavidin C1 DynaBeads (25 µL per reaction) were washed three times in 1x Bind/Wash buffer (1 M NaCl, 1mM EDTA, 10mM Tris, pH 8.0). Beads were then resuspended in 2x Bind/Wash buffer (10 µL per reaction). Beads were added to each cDNA/oligo mixture and incubated for 15 minutes at 37 °C in an Eppendorf ThermoMixer at 1000 rpm. Beads were collected on a magnetic stand and ~17.5 µL of eluate was recovered for each reaction. Resulting eluate was then used as a template for PCR amplification.

Pilot PCR reactions were prepared in order to determine the number of cycles necessary for adequate amplification. PCR reactions consisted of 20 µL of 5x HF buffer, 2 µL of 10mM dNTPs, 0.5 µL of 100 µM NI-NI-2 primer, 0.5 µL of 100 µM indexing primer (Supplementary file 1), 5 µL of eluate template, 71 µL of water and 1 µL of Phusion polymerase (NEB cat# M0530L). Each 100 µL reaction was separated into 5 16.7 µL aliquots. PCR conditions were as follows: initial denaturation for 30 seconds at 98°C, followed by cycles of 10 seconds at 98°C, 10 seconds of annealing at 65 °C, and 5 seconds of extension at 72°C. One aliquot was removed after 8,10,12, and 14 cycles. Amplification was examined by gel electrophoresis on an 8% TBE polyacrylamide gel. Once optimal cycle was determined, an additional 100 µL PCR was performed and run on an 8% TBE polyacrylamide gel. The product band was then cut out and DNA extracted from the gel slice. Libraries were quantified by Bioanalyzer using a DNA High Sensitivity kit (Agilent cat# 5067-4626). Libraries were then sequenced on an Illumina Genome Analyzer 2 according to manufacturer's instructions by the Stanford Functional Genomics Facility.

Sequence alignment and analysis

Cloning linker sequences were trimmed from Illumina reads and the trimmed fasta sequences were aligned to *S. cerevisiae* ribosomal and noncoding RNA sequences using bowtie v. 0.12.7 or v. 1.0.0 to remove rRNA reads (Langmead et al., 2009). The non-rRNA reads were aligned to the *S. cerevisiae* genome as a first pass to remove any reads that mapped to multiple locations. Reads that passed this filter (those that mapped uniquely to the genome, or those that did not map at all, such as splice junction reads) were then aligned to the S. cerevisiae transcriptome with bowtie, allowing two mismatches and only reporting alignments of reads that mapped uniquely in the transcriptome (bowtie -v 2 -m 1 -a --norc --best –strata).

The *S. cerevisae* transcriptome sequences were based on CDS sequences downloaded from the UCSC genome browser, sacCer2 assembly, in August 2011. Untranslated region coordinates were taken from supplemental table S4 of

(Nagalakshmi et al., 2008). When no UTR was annotated, 50 nt upstream and/or downstream of the CDS was included by default.

A list of read counts and read lengths per nucleotide position in the transcriptome, based on the 5' end of the mapped read, was generated. From that list, metagene grids as in Figure 2A were made by tabulating all footprints 11-36 nt long within the following regions: last 25 nt of 5' UTR, first 200 nt of CDS, last 100 nt of CDS, and first 50 nt of 3' UTR, for all genes with a CDS of at least 300 nt.

Per-codon analysis

Non-unique positions in the transcriptome were filtered by splitting the yeast transcriptome into all overlapping 20mers, mapping this set of all 20mers back to the transcriptome with bowtie, and collecting the mapped locations of any 20mers with more than one perfect match in the transcriptome.

The counts of small and large footprints from ribosomes with each codon positioned in the inferred A site were generated from the list of reads at each nucleotide position as depicted in Figure 2F. The large footprints were defined as 28 nt reads with the 5' end 15 nt upstream of the codon at position *i*, and 29 nt reads with the 5' end 16 nt upstream of *i*. Small footprints included 20 nt and 21 nt reads with the 5' end 15 nt upstream of *i* and 21 nt and 22 nt reads with the 5' end 16 nt upstream of *i*. For each gene, the analysis included codons 51 through the second codon before the stop codon, to avoid the region at the beginning of genes from which ribosomes have been depleted by runoff elongation during harvest. Genes with fewer than 10 footprints in total were excluded, as were any non-unique positions within genes.

The "relative occupancy" per codon was generated by first computing the average number of footprints (large + small) across the gene. Then, at each position *i* in gene *g*, compute (large + small at position *i*)/(average large + small in gene *g*). These ratios were then averaged across all instances of a given codon (eg, CGA) in the transcriptome to give the relative occupancy.

The densities of small and large footprints were computed as above: (small at *i*)/(average large + small in gene *g*) and similarly (large at *i*)/(average large + small in gene *g*).

Acknowledgements

We thank Nicholas Ingolia, Harry Noller, and Jody Puglisi for helpful discussion.

Competing interests

The authors declare that no competing interests exist.

References

Agirrezabala, X., Lei, J., Brunelle, J.L., Ortiz-Meoz, R.F., Green, R., and Frank, J. (2008). Visualization of the hybrid state of tRNA binding promoted by spontaneous ratcheting of the ribosome. Mol Cell *32*, 190-197.

Barbacid, M., and Vazquez, D. (1974). (3H)anisomycin binding to eukaryotic ribosomes. J Mol Biol *84*, 603-623.

Barbacid, M., and Vazquez, D. (1975). Ribosome changes during translation. J Mol Biol *93*, 449-463.

Ben-Shem, A., Garreau de Loubresse, N., Melnikov, S., Jenner, L., Yusupova, G., and Yusupov, M. (2011). The structure of the eukaryotic ribosome at 3.0 A resolution. Science *334*, 1524-1529.

Ben-Shem, A., Jenner, L., Yusupova, G., and Yusupov, M. (2010). Crystal structure of the eukaryotic ribosome. Science *330*, 1203-1209.

Charneski, C.A., and Hurst, L.D. (2013). Positively charged residues are the major determinants of ribosomal velocity. PLoS Biol *11*, e1001508.

Chen, J., Tsai, A., O'Leary, S.E., Petrov, A., and Puglisi, J.D. (2012). Unraveling the dynamics of ribosome translocation. Curr Opin Struct Biol *22*, 804-814.

Dale, T., Fahlman, R.P., Olejniczak, M., and Uhlenbeck, O.C. (2009). Specificity of the ribosomal A site for aminoacyl-tRNAs. Nucleic Acids Res *37*, 1202-1210.

Dana, A., and Tuller, T. (2012). Determinants of translation elongation speed and ribosomal profiling biases in mouse embryonic stem cells. PLoS Comput Biol *8*, e1002755.

dos Reis, M., Savva, R., and Wernisch, L. (2004). Solving the riddle of codon usage preferences: a test for translational selection. Nucleic Acids Res *32*, 5036-5044.

Ermolenko, D.N., Cornish, P.V., Ha, T., and Noller, H.F. (2013). Antibiotics that bind to the A site of the large ribosomal subunit can induce mRNA translocation. RNA *19*, 158-166.

Frank, J., and Agrawal, R.K. (2000). A ratchet-like inter-subunit reorganization of the ribosome during translocation. Nature *406*, 318-322.

Fredrick, K., and Noller, H.F. (2003). Catalysis of ribosomal translocation by sparsomycin. Science *300*, 1159-1162.

Fu, J., Munro, J.B., Blanchard, S.C., and Frank, J. (2011). Cryoelectron microscopy structures of the ribosome complex in intermediate states during tRNA translocation. Proc Natl Acad Sci U S A *108*, 4817-4821.

Gao, Y.G., Selmer, M., Dunham, C.M., Weixlbaumer, A., Kelley, A.C., and Ramakrishnan, V. (2009). The structure of the ribosome with elongation factor G trapped in the posttranslocational state. Science *326*, 694-699.

Grollman, A.P. (1967). Inhibitors of protein biosynthesis. II. Mode of action of anisomycin. J Biol Chem *242*, 3226-3233.

Guydosh, N.R., and Green, R. (2014). Dom34 rescues ribosomes in 3' untranslated regions. Cell *156*, 950-962.

Hansen, J.L., Moore, P.B., and Steitz, T.A. (2003). Structures of five antibiotics bound at the peptidyl transferase center of the large ribosomal subunit. J Mol Biol *330*, 1061-1075.

Ingolia, N.T., Brar, G.A., Rouskin, S., McGeachy, A.M., and Weissman, J.S. (2012). The ribosome profiling strategy for monitoring translation in vivo by deep sequencing of ribosome-protected mRNA fragments. Nat Protoc *7*, 1534-1550.

Ingolia, N.T., Ghaemmaghami, S., Newman, J.R., and Weissman, J.S. (2009). Genome-wide analysis in vivo of translation with nucleotide resolution using ribosome profiling. Science *324*, 218-223.

Ingolia, N.T., Lareau, L.F., and Weissman, J.S. (2011). Ribosome profiling of mouse embryonic stem cells reveals the complexity and dynamics of mammalian proteomes. Cell *147*, 789-802.

Johansson, M.J., Esberg, A., Huang, B., Bjork, G.R., and Bystrom, A.S. (2008). Eukaryotic wobble uridine modifications promote a functionally redundant decoding system. Mol Cell Biol *28*, 3301-3312.

Kapp, L.D., and Lorsch, J.R. (2004). The molecular mechanics of eukaryotic translation. Annu Rev Biochem *73*, 657-704.

Langmead, B., Trapnell, C., Pop, M., and Salzberg, S.L. (2009). Ultrafast and memory-efficient alignment of short DNA sequences to the human genome. Genome Biol *10*, R25.

Letzring, D.P., Dean, K.M., and Grayhack, E.J. (2010). Control of translation efficiency in yeast by codon-anticodon interactions. RNA *16*, 2516-2528.

Moazed, D., and Noller, H.F. (1989). Intermediate states in the movement of transfer RNA in the ribosome. Nature *342*, 142-148.

Munro, J.B., Altman, R.B., O'Connor, N., and Blanchard, S.C. (2007). Identification of two distinct hybrid state intermediates on the ribosome. Mol Cell *25*, 505-517.

Nagalakshmi, U., Wang, Z., Waern, K., Shou, C., Raha, D., Gerstein, M., and Snyder, M. (2008). The transcriptional landscape of the yeast genome defined by RNA sequencing. Science *320*, 1344-1349.

Noeske, J., and Cate, J.H. (2012). Structural basis for protein synthesis: snapshots of the ribosome in motion. Curr Opin Struct Biol *22*, 743-749.

Olejniczak, M., Dale, T., Fahlman, R.P., and Uhlenbeck, O.C. (2005). Idiosyncratic tuning of tRNAs to achieve uniform ribosome binding. Nat Struct Mol Biol *12*, 788-793.

Percudani, R., Pavesi, A., and Ottonello, S. (1997). Transfer RNA gene redundancy and translational selection in Saccharomyces cerevisiae. J Mol Biol *268*, 322-330.

Plotkin, J.B., and Kudla, G. (2011). Synonymous but not the same: the causes and consequences of codon bias. Nat Rev Genet *12*, 32-42.

Pulk, A., and Cate, J.H. (2013). Control of ribosomal subunit rotation by elongation factor G. Science *340*, 1235970.

Ratje, A.H., Loerke, J., Mikolajka, A., Brunner, M., Hildebrand, P.W., Starosta, A.L., Donhofer, A., Connell, S.R., Fucini, P., Mielke, T.*, et al.* (2010). Head swivel on the ribosome facilitates translocation by means of intra-subunit tRNA hybrid sites. Nature *468*, 713-716.

Schneider-Poetsch, T., Ju, J., Eyler, D.E., Dang, Y., Bhat, S., Merrick, W.C., Green, R., Shen, B., and Liu, J.O. (2010). Inhibition of eukaryotic translation elongation by cycloheximide and lactimidomycin. Nat Chem Biol *6*, 209-217.

Shah, P., Ding, Y., Niemczyk, M., Kudla, G., and Plotkin, J.B. (2013). Rate-limiting steps in yeast protein translation. Cell *153*, 1589-1601.

Shepotinovskaya, I., and Uhlenbeck, O.C. (2013). tRNA residues evolved to promote translational accuracy. RNA *19*, 510-516.
Stadler, M., and Fire, A. (2011). Wobble base-pairing slows in vivo translation elongation in metazoans. RNA *17*, 2063-2073.
Steitz, J.A. (1969). Polypeptide chain initiation: nucleotide sequences of the three ribosomal binding sites in bacteriophage R17 RNA. Nature *224*, 957-964.
Tourigny, D.S., Fernandez, I.S., Kelley, A.C., and Ramakrishnan, V. (2013). Elongation factor G bound to the ribosome in an intermediate state of translocation. Science *340*, 1235490.
Tuller, T., Carmi, A., Vestsigian, K., Navon, S., Dorfan, Y., Zaborske, J., Pan, T., Dahan, O., Furman, I., and Pilpel, Y. (2010). An evolutionarily conserved mechanism for controlling the efficiency of protein translation. Cell *141*, 344-354.
Wolfenden, R. (2007). Experimental measures of amino acid hydrophobicity and the topology of transmembrane and globular proteins. J Gen Physiol *129*, 357-362.
Wolin, S.L., and Walter, P. (1988). Ribosome pausing and stacking during translation of a eukaryotic mRNA. EMBO J *7*, 3559-3569.
Zhang, W., Dunkle, J.A., and Cate, J.H. (2009). Structures of the ribosome in intermediate states of ratcheting. Science *325*, 1014-1017.
Zhou, J., Lancaster, L., Donohue, J.P., and Noller, H.F. (2013). Crystal structures of EF-G-ribosome complexes trapped in intermediate states of translocation. Science *340*, 1236086.

Figure Legends

Figure 1. Schematic representation of the eukaryotic elongation cycle. Blue overlay denotes stages at which the ribosome has undergone a large inter-subunit rotation. Ribosome shapes are for illustration only, not a literal representation of the structure or degree of rotation.

Figure 2. Ribosome-protected fragment positions and size distributions from yeast not treated with elongation inhibitors. (A) The position of each fragment was calculated relative to the start codon of its gene. The 5' end positions (x axis) and lengths of all fragments (y axis) were tallied across all genes with a coding region of at least 300 nt. Higher color intensity reflects more fragments. RNA fragments between 18 and 32 nucleotides were selected after gel electrophoresis; shorter and longer fragments are not entirely excluded but their read counts are presumed to be unrepresentative of their true abundance. (B) Profiles of the 5' end positions of all 20 nt and 28 nt fragments relative to the start codon of their genes, as in (A). (C) Total counts of mapped fragment lengths. (D) Distribution of 21 nt and 28 nt fragments in coding regions and untranslated regions of mRNAs. (E) Positions of 21 nt and 28 nt fragments relative to the reading frame. (F) Interpretation of fragment positions on an arbitrary gene fragment. Arrowheads show hypothetical nuclease cleavage sites relative to a ribosome in a non-rotated or rotated conformation (shape is for illustration only). The resulting fragments are shown with the inferred decoding site (A site), and their positions in a grid as in Figure 2A are shown with corresponding colors.

Figure 2 – Figure Supplement 1. Two biological replicates of ribosome-protected fragment distribution, as in Figure 2A and 2C.

Figure 3. Ribosome-protected fragment positions and size distributions from yeast treated with elongation inhibitors. (A) and (B) As in Figure 2A and 2B, fragment position and size distribution for yeast treated with cycloheximide. (C) Distribution of mapped fragment lengths for yeast treated with cycloheximide. (D) and (E) Fragment position and size distribution for yeast treated with anisomycin. (E) Distribution of mapped fragment lengths for yeast treated with anisomycin.

Figure 3 – Figure Supplement 1. (A) Biological replicate of ribosome-protected fragment distribution after cycloheximide treatment. (B) Biological replicate (top) and technical replicate (bottom; independent fractionation and library preparation from the same lysate as Figure 3) of fragment distribution after anisomycin treatment.

Figure 4. Effect of 3-amino 1,4 triazole on translation of histidine codons. (A) Schematic representation of the hypothesized effect of 3-AT. 3-AT reduces intracellular concentrations of histidyl-tRNA and thus is expected to increase time spent decoding histidine codons (*i.e.*, in the decoding phase of the cycle, with a His codon in the A-site). (B) All 61 sense codons are plotted by the $\log_2$ of the relative abundance of large footprints with the specified codon in the A-site for untreated

682 cells (x axis) against the $\log_2$ relative abundance of large footprints for yeast treated
683 with 3-AT (y axis). Values shown are the average of three untreated replicates and
684 two 3-AT treatments (10 min and 60 min). Histidine codons are denoted in red
685 (CAT) and cyan (CAC). (C) As in (B), showing the relative abundance of small
686 footprints.

687 **Figure 4 – Figure Supplement 1.** As in figure 4, $\log_2$ relative occupancy, $\log_2$ large
688 footprint abundance, and $\log_2$ small footprint abundance in comparisons of three
689 untreated replicates and two 3-AT treated samples. Histidine codons are denoted in
690 red (CAT) and cyan (CAC).

691 **Figure 5.** Codon-specific variation in large and small footprint abundance. (A)
692 Distribution of ribosome footprint counts on the highly expressed gene FBA1,
693 highlighting an arbitrary window, codons 250-279. Ribosome footprint counts per
694 position were consistent between replicates and varied between instances of the
695 same codon in this window. Relative occupancy was estimated based on the codon
696 in the inferred A site. Total (large + small) footprint coverage at each codon of a
697 gene was computed relative to the average coverage for that gene, then averaged by
698 codon across all genes to provide per-codon relative occupancies. Relative
699 abundance of small or large footprints was computed similarly, comparing the count
700 of small or large footprints at each codon of a gene against the average coverage
701 (large + small) for that gene, then averaged by codon across all genes. Examples of
702 small and large footprint abundance values at two specific TTC codons in FBA1 are
703 shown. (B) Relative occupancies of all 61 codons compared between two replicates,
704 with Spearman correlation of 0.81. Stop codons and the first 50 codons of each gene
705 were excluded from analysis. Similarly, small footprint abundance (C) and large
706 footprint abundance (D) compared between replicates.

707 **Figure 5 – Figure Supplement 1.** (A) Relative occupancies based on the codon
708 downstream of the inferred A site, compared to the A-site occupancies as in figure 5.
709 Similarly, small footprint abundance (B) and large footprint abundance (C) for the
710 inferred A site and downstream codon.

711 **Figure 6.** Correlates of footprint abundance. (A) Small footprint abundance,
712 averaged for all codons encoding the same amino acid plotted against K_d of transfer
713 of side chain from vapor to water as a measure of polarity (Wolfenden, 2007), with
714 Spearman correlation from the average of three samples. (B) Relative occupancy of
715 directly paired codons versus relative occupancy of codons that recognize the same
716 tRNA with wobble pairing. Values are the average of three replicates. Dashed line
717 shows y=x, the expected relationship if occupancy were determined solely by tRNA
718 identity. (C,D) As in (B), showing small and large footprint abundance.

719 **Supplementary file 1.** Primer sequences.

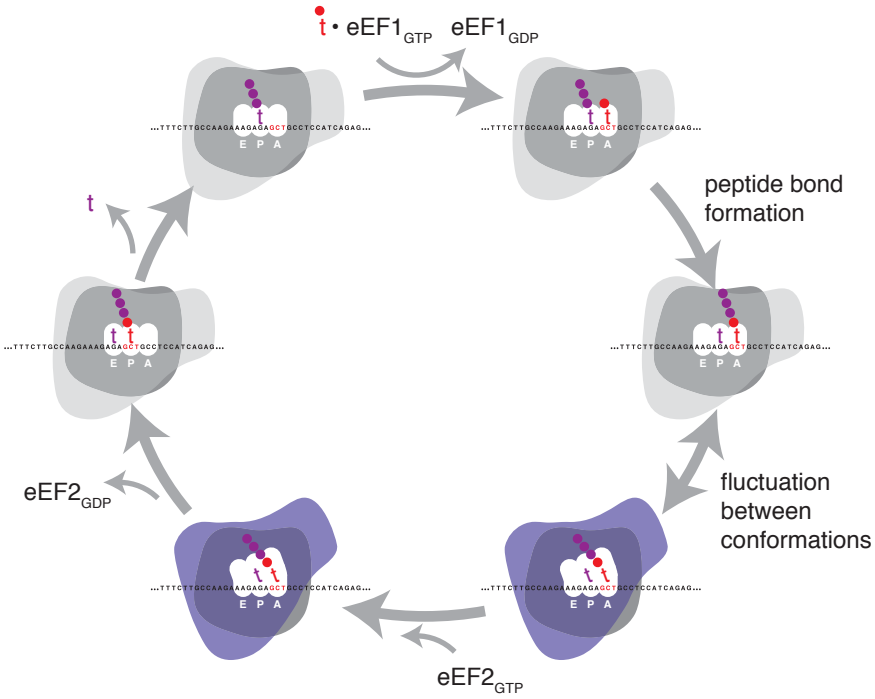
t • eEF1GTP
eEF1GDP
peptide bond formation
fluctuation between conformations
eEF2GTP
eEF2GDP
t
E P A

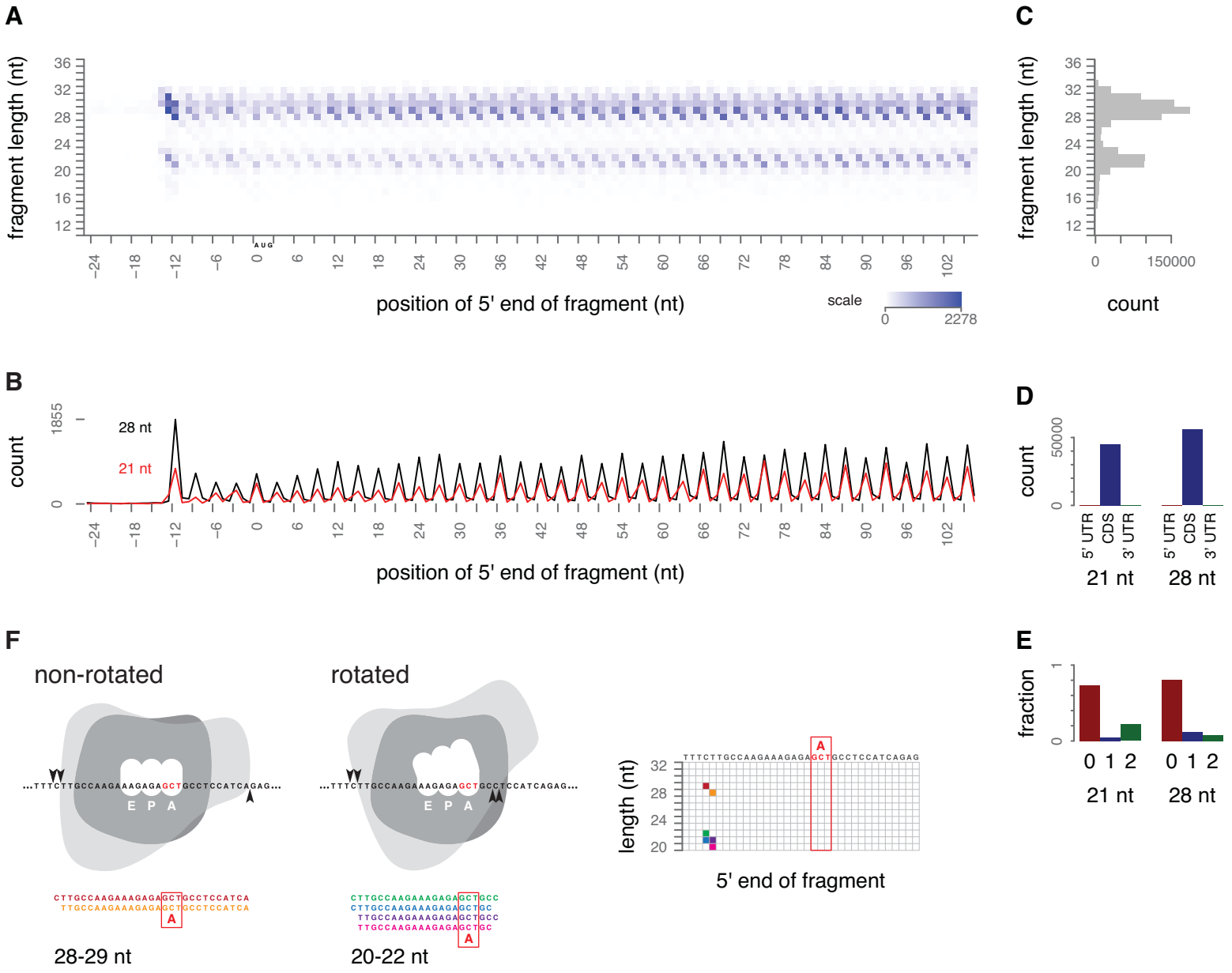
A
fragment length (nt)
position of 5' end of fragment (nt)
scale
0
2278
C
fragment length (nt)
count
B
count
28 nt
21 nt
position of 5' end of fragment (nt)
D
count
5' UTR
CDS
3' UTR
21 nt
28 nt
F
non-rotated
rotated
E P A
28-29 nt
20-22 nt
length (nt)
5' end of fragment
E
fraction
0 1 2
21 nt
28 nt

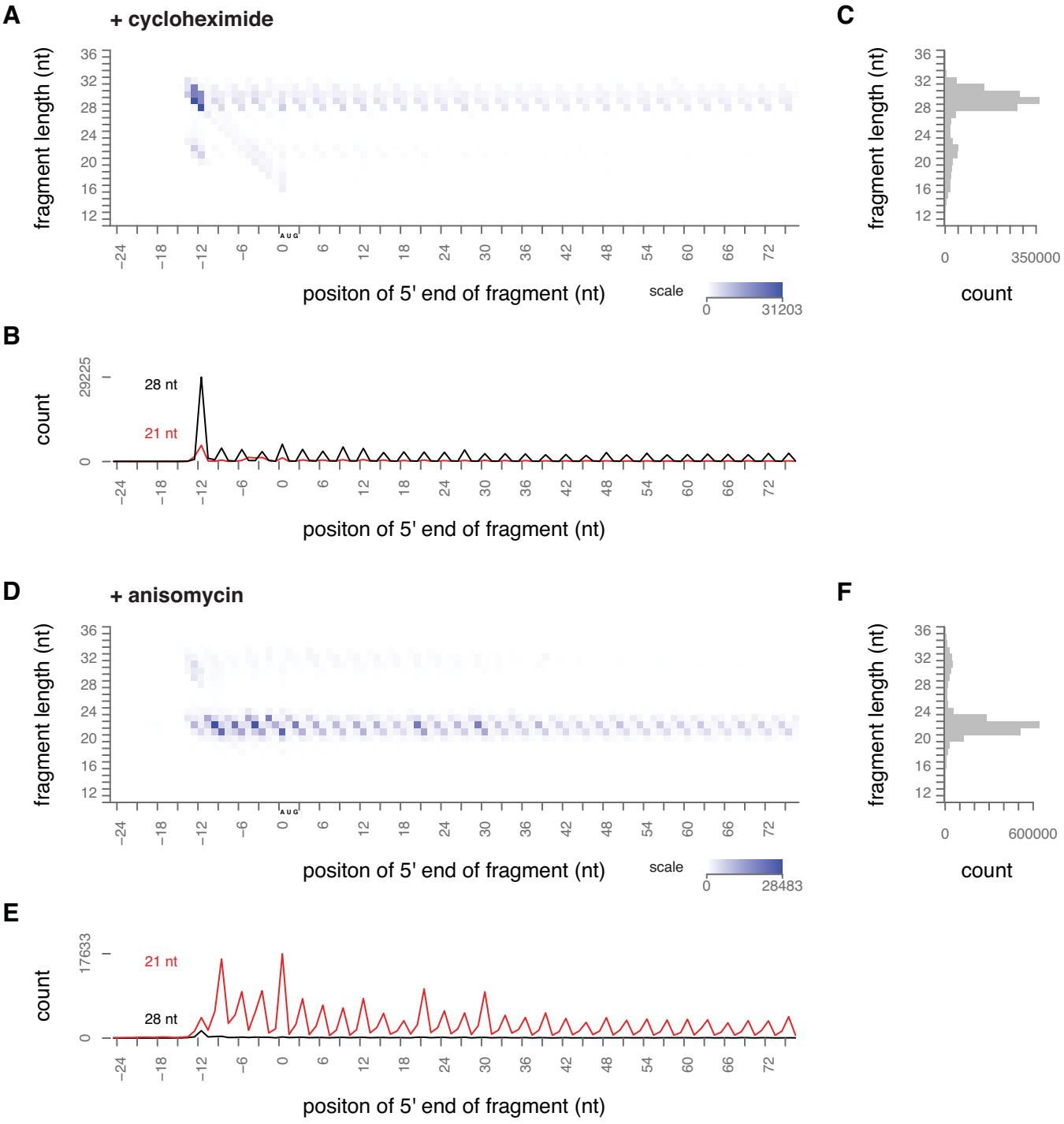
A
+ cycloheximide
fragment length (nt)
positon of 5' end of fragment (nt)
scale
0
31203
C
fragment length (nt)
count
0
350000
B
count
29225
28 nt
21 nt
positon of 5' end of fragment (nt)
D
+ anisomycin
fragment length (nt)
positon of 5' end of fragment (nt)
scale
0
28483
F
fragment length (nt)
count
0
600000
E
count
17633
21 nt
28 nt
positon of 5' end of fragment (nt)

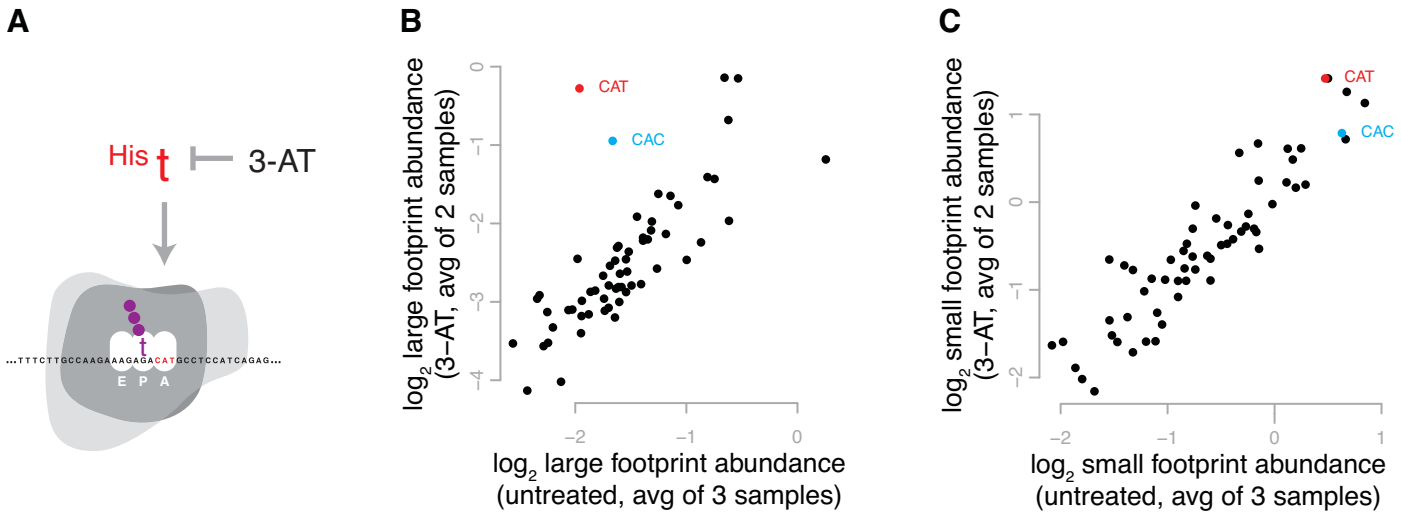
A
His
t
3-AT
...TTTCTTGCCAAGAAAGAGACATGCCTCCATCAGAG...
E P A
B
log2 large footprint abundance
(3–AT, avg of 2 samples)
CAT
CAC
log2 large footprint abundance
(untreated, avg of 3 samples)
C
log2 small footprint abundance
(3–AT, avg of 2 samples)
CAT
CAC
log2 small footprint abundance
(untreated, avg of 3 samples)

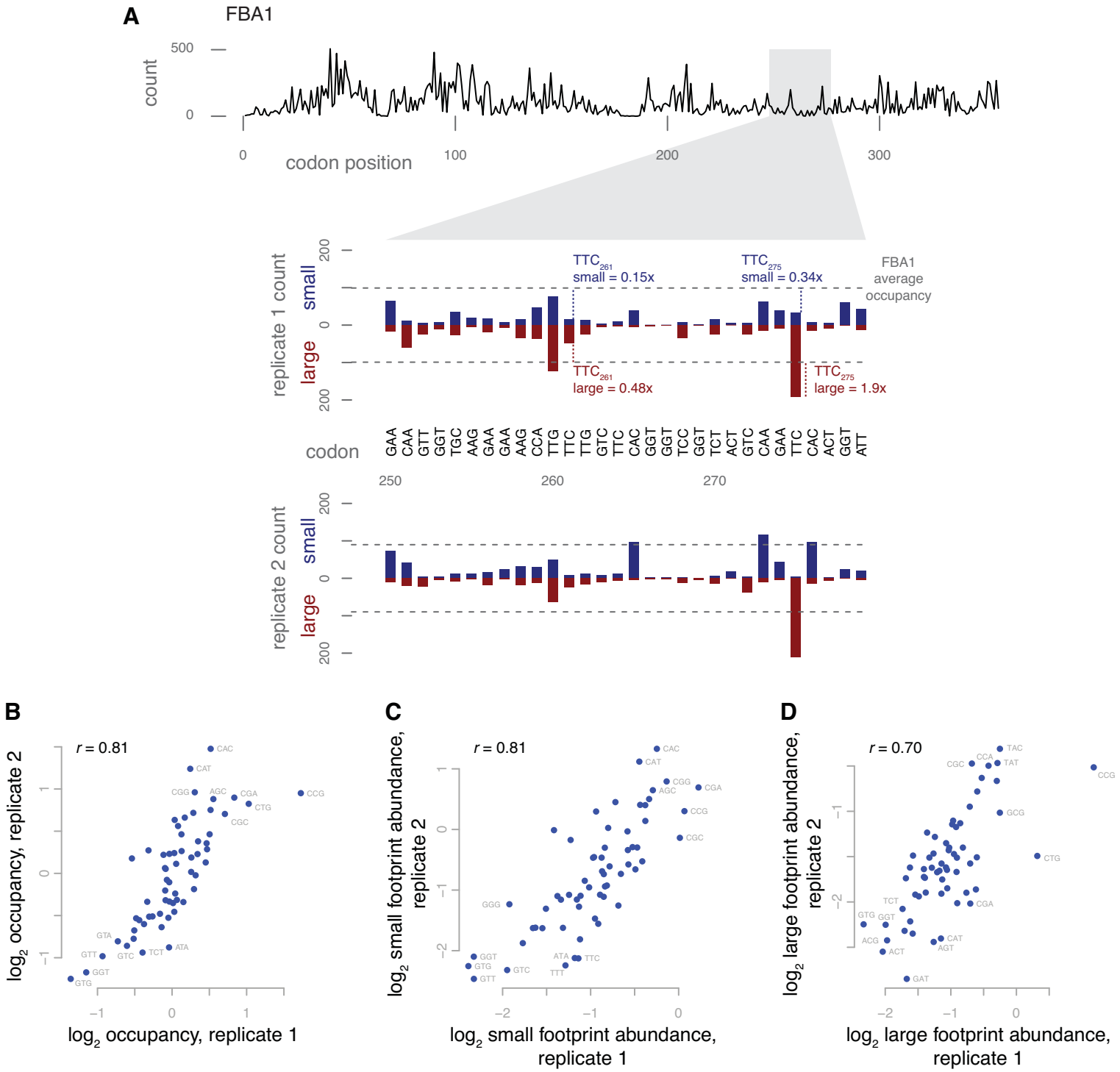
A
FBA1
count
500
0
0
codon position
100
200
300
replicate 1 count
small
large
200
0
200
TTC261
small = 0.15x
TTC275
small = 0.34x
FBA1
average
occupancy
TTC261
large = 0.48x
TTC275
large = 1.9x
codon
GAA CAA GTT GGT TGC AAG GAA GAA AAG CCA TTG TTC TTG GTC TTC CAC GGT GGT TCC GGT TCT ACT GTC CAA GAA TTC CAC ACT GGT ATT
250
260
270
replicate 2 count
small
large
200
0
200
B
r = 0.81
log2 occupancy, replicate 2
log2 occupancy, replicate 1
C
r = 0.81
log2 small footprint abundance, replicate 2
log2 small footprint abundance, replicate 1
D
r = 0.70
log2 large footprint abundance, replicate 2
log2 large footprint abundance, replicate 1

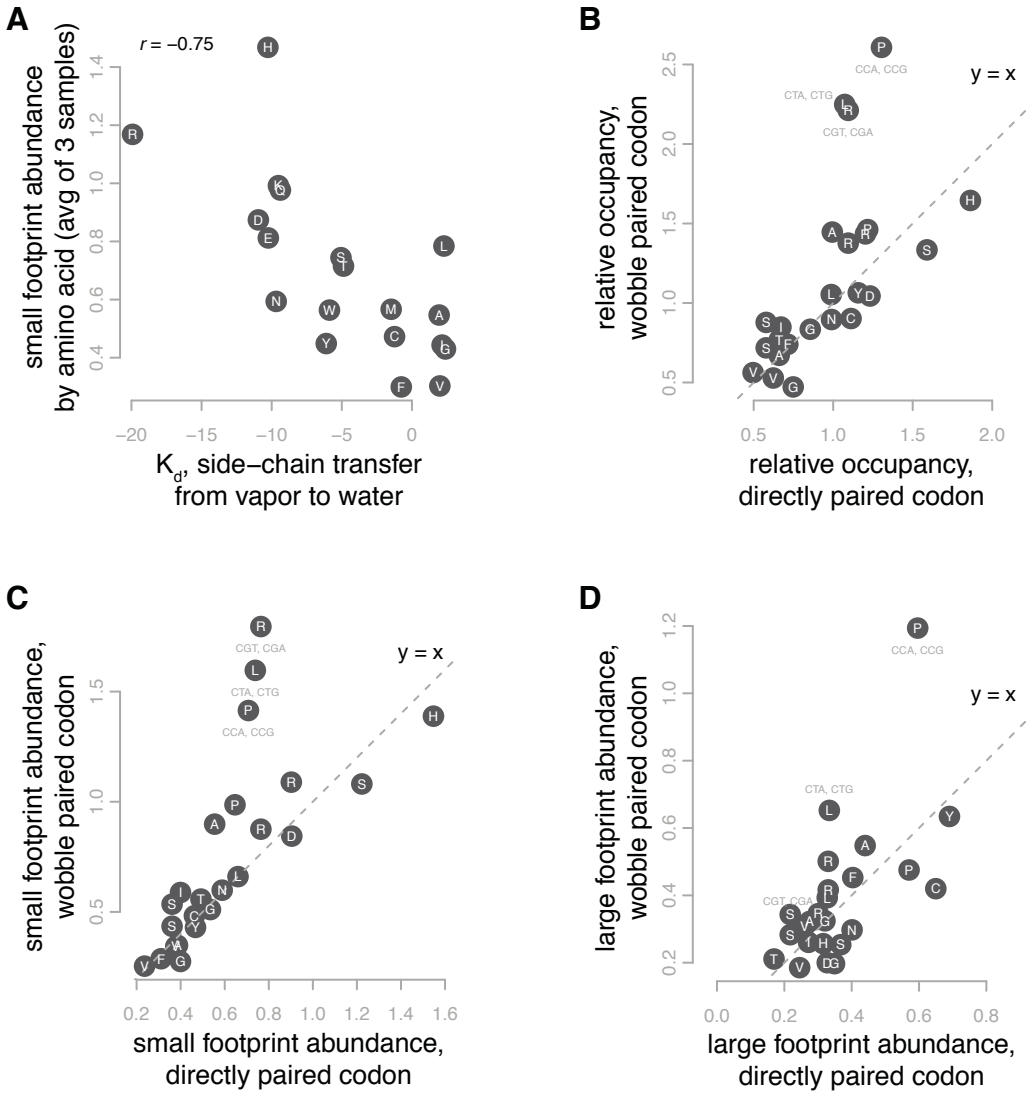
A
r = −0.75
small footprint abundance
by amino acid (avg of 3 samples)
0.4
0.6
0.8
1.0
1.2
1.4
−20
−15
−10
−5
0
K_d, side−chain transfer
from vapor to water
B
y = x
CCA, CCG
CTA, CTG
CGT, CGA
relative occupancy,
wobble paired codon
0.5
1.0
1.5
2.0
2.5
relative occupancy,
directly paired codon
C
y = x
CGT, CGA
CTA, CTG
CCA, CCG
small footprint abundance,
wobble paired codon
0.5
1.0
1.5
0.2
0.4
0.6
0.8
1.0
1.2
1.4
1.6
small footprint abundance,
directly paired codon
D
y = x
CCA, CCG
CTA, CTG
CGT, CGA
large footprint abundance,
wobble paired codon
0.2
0.4
0.6
0.8
1.0
1.2
0.0
0.2
0.4
0.6
0.8
large footprint abundance,
directly paired codon